ChemComm

COMMUNICATION

View Article Online
View Journal | View Issue

Cite this: *Chem. Commun.*, 2020, **56**, 12574

Received 9th July 2020,
Accepted 13th September 2020

DOI: 10.1039/d0cc04756b

rsc.li/chemcomm

Unconventional magnetism in the high pressure 'all transition metal' double perovskite Mn_2NiReO_6†‡

Elena Solana-Madruga,[a] Khalid N. Alharbi,[a] Maria Herz,[a] Pascal Manuel[b] and J. Paul Attfield *[a]

Mn_2NiReO_6, prepared at high pressure and temperature, has a highly-distorted double perovskite structure. Canted antiferromagnetic order is observed below T_{M1} = 80 K and an unusual continuous spin rotation of Mn spins occurs down to T_{M2} = 42 K where a collapse in weak ferromagnetism evidences an unprecedented switching of the weak ferromagnetic moment directions.

$A_2BB'O_6$ double perovskites with rocksalt-type order of the B/B′ cations have been of great interest since the discovery of large magnetoresistances in Sr_2FeMoO_6.[1,2] Double perovskites synthesised at ambient pressure typically have large, non-magnetic A-site cations like Ca^{2+}, Sr^{2+}, and Ba^{2+}, but a recent breakthrough has come from the discovery that Mn^{2+} analogues can be recovered from high pressures. Complex magnetic orders result from the S = 5/2 Mn^{2+} A-site cations in addition to transition metal B-cation spins. Mn_2FeSbO_6[3] (and the basic ABO_3-type perovskite $MnVO_3$-II[4]) have incommensurate helimagnetic structures. The 'All Transition Metal' (ATM) double perovskite Mn_2FeReO_6 is ferrimagnetic with a high Curie temperature of 520 K and frustration switching of spin order and magnetoresistance on cooling.[5,6] Mn_2MnReO_6 is also frustrated with perpendicular A and B site Mn^{2+} sublattices[7,8] and Mn_2CoReO_6 is antiferromagnetically ordered below 94 K.[9] Here we report the new ATM double perovskite Mn_2NiReO_6 which shows remarkable Mn^{2+} spin rotation and weak ferromagnetic properties.

Mn_2NiReO_6 was synthesised at 8 GPa and 1573 K using a Walker-type multi-anvil press. Stoichiometric proportions of MnO, NiO and ReO_3 were ground in acetone and packed into a Pt capsule. The product was quenched to room temperature and slowly depressurized. Formation of a double perovskite was confirmed using powder X-ray diffraction (XRD) from a Bruker D2-Phaser instrument, and high resolution neutron powder diffraction (NPD) data were collected using the WISH instrument at ISIS. Long NPD scans were taken at 1.5, 75, and 150 K to determine crystal and magnetic structures, and shorter scans at intermediate temperatures were used to reveal their thermal evolutions. Diffraction data were fitted using the FullProf software suite.[10] Magnetic susceptibility was measured using a superconducting quantum interference device (SQUID) Quantum Design XL-MPMS magnetometer in the temperature range 2–300 K under zero-field cooling (ZFC) and field-cooling (FC) conditions in a magnetic field of 1000 Oe. Magnetisation-field hysteresis loops were collected at 2, 60, 75 and 150 K under applied magnetic fields up to 7 T.

Mn_2NiReO_6 was found to have a monoclinic $P2_1/n$ double perovskite crystal structure from refinements against XRD and NPD data (Fig. 1 and ESI,‡ Fig. S1). Secondary phases of ReO_2, NiO and another rocksalt type phase, $Ni_{0.67}Mn_{0.33}O$[11] (17.8(6) wt%, 4.0(3) wt% and 12.2(2) wt% respectively), were also fitted. See ESI‡ for further discussion. The large contrasts in neutron scattering lengths for Mn, Ni, Re and O (−3.73, 10.3, 9.2 and 5.8 fm respectively)[12] enable accurate determination of the cation distribution and oxygen positions. Structure refinement using the 150 K NPD data, summarized in ESI,‡ Table S1, reveals that the Mn and Re sites are fully occupied but 18% Mn substitutes for Ni, so the overall chemical composition $Mn_{2.18}Ni_{0.82}ReO_6$ is in keeping with the Ni-rich impurities observed.

The interatomic distances, as summarized in Fig. 2 and Table S1 (ESI‡), show that the structure of Mn_2NiReO_6 is highly distorted from the ideal double perovskite arrangement. The A-site Mn coordination is reduced from the ideal perovskite 12-fold environment to an irregular 7-coordinate polyhedron, with Mn–O distances ranging from 1.70 to 2.83 Å (and other distances >3.10 Å, see ESI,‡ Table S5). This differs from other

[a] *Centre for Science at Extreme Conditions (CSEC) and School of Chemistry, University of Edinburgh, Mayfield Road, Edinburgh EH9 3JZ, UK. E-mail: j.p.attfield@ed.ac.uk*
[b] *ISIS Facility, Rutherford Appleton, Laboratory, Harwell, Oxford, Didcot OX11 0QX, UK*

† Data that support the findings of this study have been deposited at https://datashare.is.ed.ac.uk/handle/10283/838.

‡ Electronic supplementary information (ESI) available: Supporting figures and tables. See DOI: 10.1039/d0cc04756b

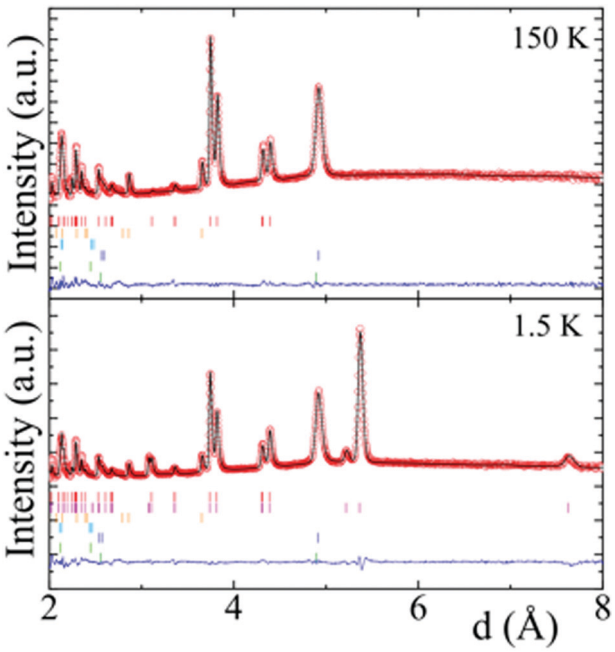

Fig. 1 Rietveld fits to 150 and 1.5 K NPD data of Mn_2NiReO_6. Bragg phase markers at 1.5 K from top to bottom are; Mn_2NiReO_6 nuclear and magnetic, ReO_2, NiO nuclear and magnetic, and (Ni,Mn)O nuclear and magnetic.

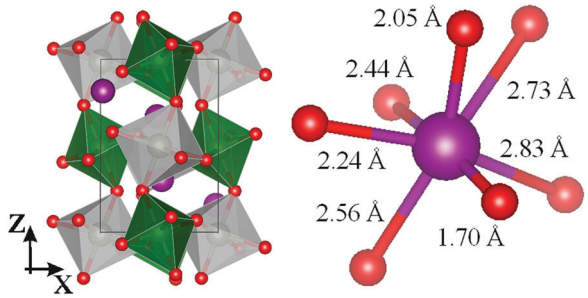

Fig. 2 Structure of the double perovskite Mn_2NiReO_6, as refined from 150 K NPD data. Mn is shown as purple spheres and Ni and Re octahedra are green and grey respectively. The coordination of Mn^{2+} in the A site is depicted on the right.

$Mn_2BB'O_6$ double perovskites where 8-coordination of Mn up to a similar distance limit was reported.[3,5–9,13–15] Mn_2NiReO_6 also has a very short Mn–O distance of 1.70 Å showing that the structure is highly distorted. (Short Mn^{2+}–O distances have also been reported in high pressure Mn_3O_4.[16]) A comparison against other $Mn_2BB'O_6$ double perovskites in ESI‡ shows that Mn_2NiReO_6 has the largest octahedral tilt angles and distortion parameters reported in this family to date. Although bond distances and derived Bond Valence Sums in ESI‡ do not distinguish clearly between Ni^{2+}/Re^{6+} and Ni^{3+}/Re^{5+} charge distributions,[17] magnetic moments refined against 1.5 K NPD data indicate Ni^{2+}/Re^{6+}, as also found in Sr_2NiReO_6.[18,19]

Temperature variation of magnetic susceptibility is shown in Fig. 3a. The Curie–Weiss fit shown gives an effective paramagnetic

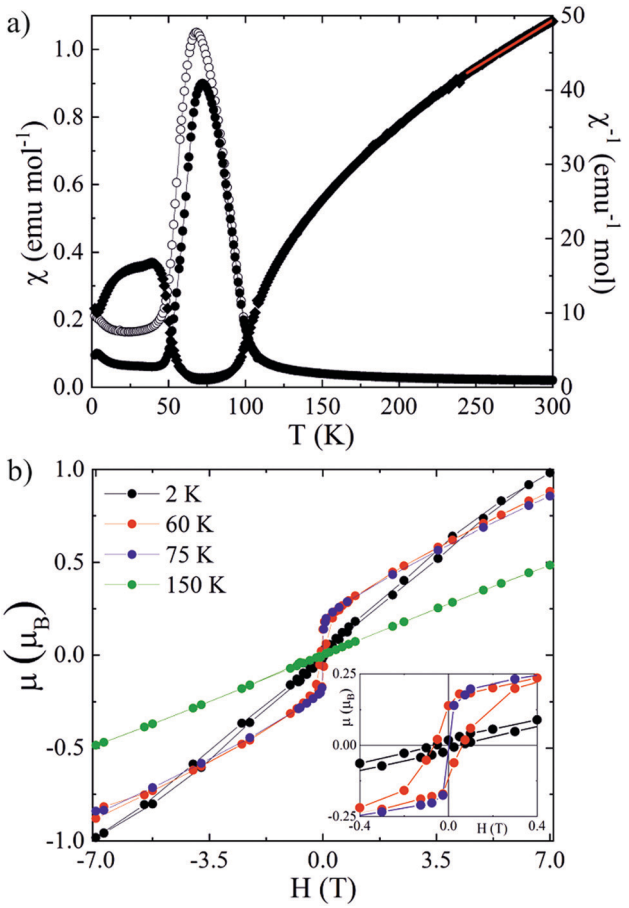

Fig. 3 (a) Magnetic susceptibility of Mn_2NiReO_6 (ZFC/FC = closed/open symbols) and the reciprocal ZFC data with Curie–Weiss fit shown. (b) Magnetisation-field hysteresis loops at several temperatures with the low field region of the spin-ordered regime in the inset.

moment of 8.16 μ_B f.u.$^{-1}$ which is comparable to the spin-only estimate of 9.0 μ_B per unit Mn_2NiReO_6, given the presence of secondary phases. The fitted Weiss constant is θ = 1.8 K but this may not be meaningful given the presence of impurities and extrapolation from a small fitting range. A sharp ferro- or ferrimagnetic transition with divergence of ZFC and FC data is observed at T_{M1} = 80 K, and a discontinuity reveals a second magnetic transition at T_{M2} = 42 K. Magnetic hysteresis loops at 60 and 75 K in Fig. 3b show a small net moment of 0.17 μ_B f.u.$^{-1}$, indicating that a weak ferromagnetic order is present below T_{M1}. However, at 2 K, below the second magnetic transition, the loop has almost collapsed with a residual moment of 0.02 μ_B f.u.$^{-1}$ although the coercive field of 51 mT is comparable to the 60 K value of 63 mT.

Magnetic peaks from Mn_2NiReO_6 are observed in neutron powder diffraction (NPD) patterns below T_{M1} = 80 K, as shown in Fig. 1 and 4. All magnetic peaks are indexed by propagation vector k = [0 0 0] and fits of different models from magnetic symmetry analysis[10] showed that the Mn, Ni, and Re spins all follow the same irreducible representation corresponding to antiferromagnetic order of spins in the *ac*-plane, as shown in Fig. 4a. All moments are ordered below 80 K. Ni^{2+} and Re^{6+} site

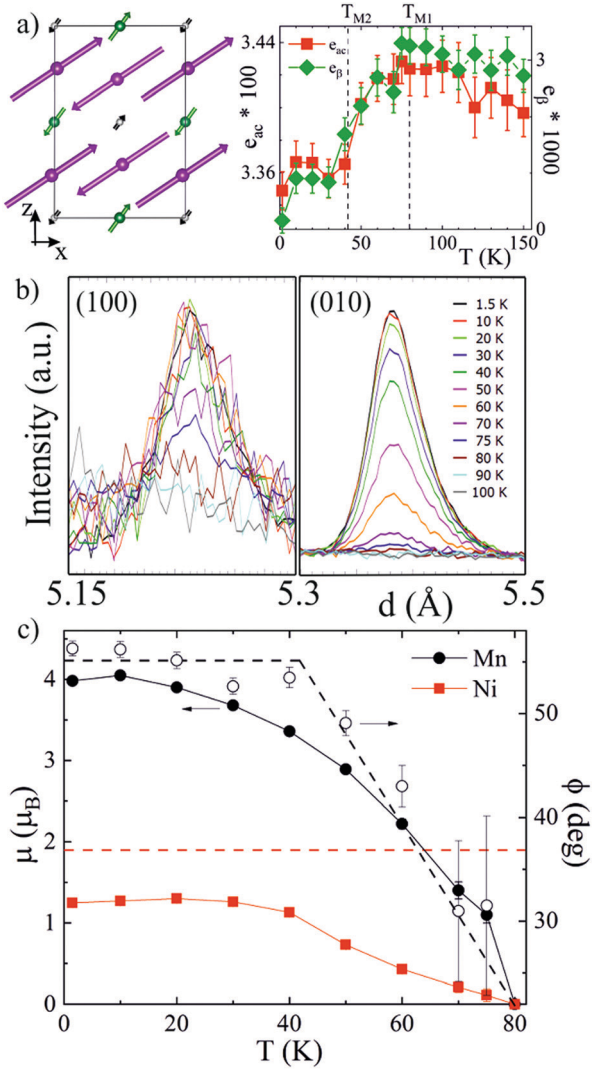

Fig. 4 (a) Magnetic structure of Mn_2NiReO_6 at 1.5 K. The right panel shows the thermal variation strain of the e_{ac} and e_b parameters. (b) Plots of (100) and (010) magnetic peaks showing their different thermal evolutions. K. (c) Thermal evolution of the refined magnetic moments and angles ϕ (closed and open symbols, respectively) for Mn^{2+} and Ni^{2+} site spins. Re^{6+} moments were constrained to take half the value of those for Ni^{2+}.

moments were found to have magnitudes in a ratio near 2 : 1 and were constrained to this ratio following their ideal S values for stability of the magnetic fits. Full refinement of the crystal and magnetic structures at 1.5 K gave respective moments of 3.98(3), 1.25(1) and 0.62 μ_B for Mn^{2+}, Ni^{2+} and Re^{6+}. These are lower than their ideal 5, 2 and 1 μ_B values evidencing the magnetic frustration within the highly connected networks of the three magnetic cations as well as the Ni/Mn disorder. Magnetic moments for 5d cations are also known to be reduced by effects of large spin–orbit coupling and strong hybridization with oxygen.[20–22]

The magnetic structure of Mn_2NiReO_6 has moments coupled parallel in the c-direction but antiparallel in the ab-plane through Ni–O–Re and Mn–O–Mn linkages, demonstrating the presence of competing ferro- and anti-ferromagnetic interactions, in keeping with the small Weiss temperature. In an ideal, undistorted, double perovskite, 180° M–O–M′ superexchange interactions between t_{2g}^1 Re^{6+} and $t_{2g}^6e_g^2$ Ni^{2+} are expected to be ferromagnetic whereas couplings between $t_{2g}^3e_g^2$ Mn^{2+} ions would be antiferromagnetic, and a variety of 90° M–O–M′ interactions are also present.

Magnetic peaks intensities from Mn_2NiReO_6 are found to evolve differently on cooling, for example, the (100) peak shown in Fig. 4b is essentially saturated below ~50 K, while the (010) intensity continues to grow down to 10 K. This demonstrates that spin components parallel to these planes grow at different rates, and refinements showed that spin rotation occurs in the ac-plane as the spin order saturates. Initial fits showed that the spin direction for Ni (and Re) sites does not change significantly with temperature, and so in the final fits, the Ni (and Re) spin direction was fixed while the Mn x- and z-components were refined independently (see ESI‡ for details). The resulting moments and rotation angles ϕ (defined as the angle of rotation from $+c$ towards $+a$ in the xz-plane) are shown in Fig. 4c. The monoclinic symmetry of Mn_2NiReO_6 enables the sign of the rotation angles ϕ to be determined.

The thermal variation of spin angles in Fig. 4c shows that Mn spins initially order with $\phi_{Mn} \approx 30°$ just below T_{M1} = 80 K. This is within error of the constant $\phi_B = 36°$ tilt angle that the ordered Ni and Re site moments exhibit at all temperatures, so all spins are essentially collinear just below T_{M1}. The tilts of the NiO_6 and ReO_6 octahedra are respectively $\psi_{Ni} = -\psi$ and $\psi_{Re} = +\psi$, following the same sign convention as for the spin rotation angles ϕ, where the octahedral tilt angle is $\psi = 23°$ as shown in ESI.‡ The opposite signs of ψ_{Ni} and ψ_{Re} result from their out-of-phase tilting in the z-direction (Fig. 2). Hence all ordered spins are near parallel to the tilted axis of the ReO_6 octahedra immediately below T_{M1}. This likely results from the strong electronic anisotropy of $5d^1$ Re^{6+}, as $3d^8$ Ni^{2+} and high spin $3d^5$ Mn^{2+} both have non-degenerate ground states.

Although spin reorientation transitions, where spin directions switch from one fixed direction to another, are known in double perovskites, *e.g.* Sr_2CoOsO_6,[20] continuous changes of spin direction over a broad temperature range do not usually occur. Spin directions remain fixed in all of the previously reported $Mn_2BB'O_6$ double perovskites shown in ESI‡ except for the reorientation transition in Mn_2FeReO_6.[6] However, the Mn spin angle ϕ_{Mn} in Mn_2NiReO_6 increases continuously from $\phi_{Mn} \approx 30°$ just below T_{M1} = 80 K to $\phi_{Mn} = 55°$ at T_{M2} = 42 K. ϕ_{Mn} is effectively constant below T_{M2}, so the second transition marks a change between rotating and non-rotating Mn^{2+} spin phases. This is most likely driven by frustration between the spin orders. Each Mn spin is surrounded by two 'up' and two 'down' Ni and Re spins, and each Ni or Re spin has four 'up' and four 'down' Mn spin neighbours. The monoclinic lattice distortion breaks the equivalence of spin–spin interactions and couples the spin orders, as evidenced by discontinuities at T_{M1} and T_{M2} in lattice strains $e_{ac} = 1 - \sqrt{2}a/c$ and $e_b = \cos\beta$ measured from the refined cell parameters (see ESI‡) observed in Fig. 4a.

Neutron diffraction reveals antiferromagnetic ordering of the Mn, Ni, and Re spins in Mn_2NiReO_6, but the magnetisation

data in Fig. 3 show that a small ferromagnetic component is also present. This is explained by the presence of non-zero antisymmetric Dzyaloshinskii–Moriya exchange interactions leading to canting of the moments. Symmetry analysis in ESI‡ shows that the irreducible representation describing the observed antiferromagnetic orders of spins in the *ac*-plane also permits ferromagnetic components in the *b* direction, although these are too small to be detected by NPD. Such weak ferromagnetism is common in perovskites where octahedral tilting lowers symmetry and can used to generate electrical polarisation and hence multiferroic properties.[23]

All three of the antiferromagnetic Mn, Ni, and Re sublattices in Mn_2NiReO_6 give rise to ferromagnetic components. It is notable that the net ferromagnetic moment takes a relatively large value $\sim 0.17\ \mu_B$ f.u.$^{-1}$ in the rotating-spin phase on cooling below T_{M1} = 80 K, but collapses to a much smaller value $\sim 0.02\ \mu_B$ f.u.$^{-1}$ approaching T_{M2} = 42 K below which spin directions are fixed. A possible explanation for this is that the relative directions of some of the ferromagnetic components switch at the T_{M2} transition. A switch from +++ directions of the respective weak ferromagnetic moments of Mn, Ni and Re spins above T_{M2}, aligned with the applied field, to +−− below, driven by antiferromagnetic coupling between the ferromagnetic *y*-components at the A and at the B, B′ sublattices as the spins become more fully ordered, accounts for the observed sharp magnetisation change at T_{M2}. Such a transition based on switching of weak ferromagnetic moments from a ferro- to a ferri-magnetic order is unprecedented and demonstrates a further new possibility generated by having magnetic A and B sublattices in 'all transition metal' perovskites.

In conclusion, the new ATM double perovskite Mn_2NiReO_6 prepared under high pressure and high temperature conditions shows a high degree of $Mn^{2+}/Ni^{2+}/Re^{6+}$ cation order although 18% excess of Mn^{2+} substitutes for Ni. The monoclinic structure of Mn_2NiReO_6 is highly distorted with the largest octahedral tilt angles and distortion parameters reported for in the $Mn_2BB'O_6$ family to date. All three magnetic sublattices order simultaneously at T_{M1} = 80 K with antiferromagnetically-oriented spins, and an unusual change between rotating and non-rotating Mn^{2+} spin phases at T_{M2} = 42 K. Weak ferromagnetism due to spin canting is observed but the net magnetisation undergoes a collapse at T_{M2}, consistent with switching of the relative directions of the weak ferromagnetic moments at the different sublattices from a ferro- to a ferrimagnetic arrangement. The unusual spin rotation, not seen in other $Mn_2BB'O_6$ analogues, and the novel switching of weak ferromagnetic states demonstrate further new possibilities that arise from interacting magnetic A and B sublattices in highly distorted 'all transition metal' double perovskite lattices.

We acknowledge EPSRC for funding and STFC for beamtime allocation at ISIS. K. N. A. acknowledges funding from King Abdulaziz City for Science and Technology (KACST).

Conflicts of interest

There are no conflicts to declare.

Notes and references

1 K.-I. Kobayashi, T. Kimura, H. Sawada, K. Terakura and Y. Tokura, *Nature*, 1998, **395**, 677–680.
2 S. Vasala and M. Karppinen, *Prog. Solid State Chem.*, 2015, **43**, 1–36.
3 A. J. Dos santos-García, C. Ritter, E. Solana-Madruga and R. Sáez-Puche, *J. Phys.: Condens. Matter*, 2013, **25**, 206004.
4 M. Markkula, A. M. Arevalo-Lopez, A. Kusmartseva, J. A. Rodgers, C. Ritter, H. Wu and J. P. Attfield, *Phys. Rev. B: Condens. Matter Mater. Phys.*, 2011, **84**, 094450.
5 M.-R. Li, M. Retuerto, Z. Deng, P. W. Stephens, M. Croft, Q. Huang, H. Wu, X. Deng, G. Kotliar, J. Sánchez-Benítez, J. Hadermann, D. Walker and M. Greenblatt, *Angew. Chem., Int. Ed.*, 2015, **54**, 12069–12073.
6 A. M. Arévalo-López, G. M. McNally and J. P. Attfield, *Angew. Chem., Int. Ed.*, 2015, **54**, 12074–12077.
7 M.-R. Li, J. P. Hodges, M. Retuerto, Z. Deng, P. W. Stephens, M. C. Croft, X. Deng, G. Kotliar, J. Sánchez-Benítez, D. Walker and M. Greenblatt, *Chem. Mater.*, 2016, **28**, 3148–3158.
8 A. M. Arévalo-López, F. Stegemann and J. P. Attfield, *Chem. Commun.*, 2016, **52**, 5558–5560.
9 C. E. Frank, E. E. McCabe, F. Orlandi, P. Manuel, X. Tan, Z. Deng, M. Croft, V. Cascos, T. Emge, H. L. Feng, S. Lapidus, C. Jin, M. X. Wu, M. R. Li, S. Ehrlich, S. Khalid, N. Quackenbush, S. Yu, D. Walker and M. Greenblatt, *Chem. Commun.*, 2019, **55**, 3331–3334.
10 J. Rodriguez-Carvajal, *Physica B*, 1993, **192**, 55–69.
11 E. Solana-Madruga, Y. Sun, A. M. Arévalo-López and J. P. Attfield, *Chem. Commun.*, 2019, **55**, 2605–2608.
12 V. F. Sears, *Neutron News*, 1992, **3**, 26–37.
13 E. Solana-Madruga, A. J. Dos santos-García, A. M. Arévalo-López, D. Ávila-Brande, C. Ritter, J. P. Attfield and R. Sáez-Puche, *Dalton Trans.*, 2015, **44**, 20441–20448.
14 A. J. Dos santos-García, E. Solana-Madruga, C. Ritter, D. Ávila-Brande, O. Fabelo and R. Sáez-Puche, *Dalton Trans.*, 2015, **44**, 10665–10672.
15 A. M. Arévalo-López, E. Solana-Madruga, C. Aguilar-Maldonado, C. Ritter, O. Mentré and J. P. Attfield, *Chem. Commun.*, 2019, **55**, 14470–14473.
16 S. Hirai, A. M. dos Santos, M. C. Shapiro, J. J. Molaison, N. Pradhan, M. Guthrie, C. A. Tulk, I. R. Fisher and W. L. Mao, *Phys. Rev. B: Condens. Matter Mater. Phys.*, 2013, **87**, 014417, distances are shown in ICSD CIF file 188903.
17 T. Stoyanova-Lyubenova, A. J. Dos santos-García, E. Urones-Garrote, M. J. Torralvo and M. Á. Alario-Franco, *Dalton Trans.*, 2014, **43**, 1117–1124.
18 H. Kato, T. Okuda, Y. Okimoto and Y. Tomioka, *Phys. Rev. B: Condens. Matter Mater. Phys.*, 2004, **69**, 184412.
19 M. Retuerto, M. J. Martínez-Lope, M. García-Hernández, M. T. Fernández-Díaz and J. A. Alonso, *Eur. J. Inorg. Chem.*, 2008, 588–595.
20 R. Morrow, R. Mishra, O. D. Restrepo, M. R. Ball, W. Windl, S. Wurmehl, U. Stockert, B. Büchner and P. M. Woodward, *J. Am. Chem. Soc.*, 2013, **135**, 18824–18830.
21 R. Morrow, J. W. Freeland and P. M. Woodward, *Inorg. Chem.*, 2014, **53**, 7983–7992.
22 P. Kayser, S. Injac, B. J. Kennedy, T. Vogt, M. Avdeev and H. E. Maynard-Casely, *Inorg. Chem.*, 2017, **56**, 6565–6575.
23 N. A. Spaldin and R. Ramesh, *Nat. Mater.*, 2019, **18**, 203–212.